JOC Article
pubs.acs.org/joc

Magnetically Induced Currents in Bianthraquinodimethane-Stabilized Möbius and Hückel [16]Annulenes

Stefan Taubert,*[,†] Dage Sundholm,*[,†] and Fabio Pichierri*[,‡]

[†]*Department of Chemistry, University of Helsinki, P.O. Box 55, A.I. Virtanens plats 1, Helsinki FIN-00014, Finland, and* [‡]*G-COE Laboratory, Department of Applied Chemistry, Graduate School of Engineering, Tohoku University, Aoba-yama 6-6-07, Sendai 980-8579, Japan*

stefan.taubert@helsinki.fi; sundholm@chem.helsinki.fi; fabio@che.tohoku.ac.jp

Received April 7, 2009

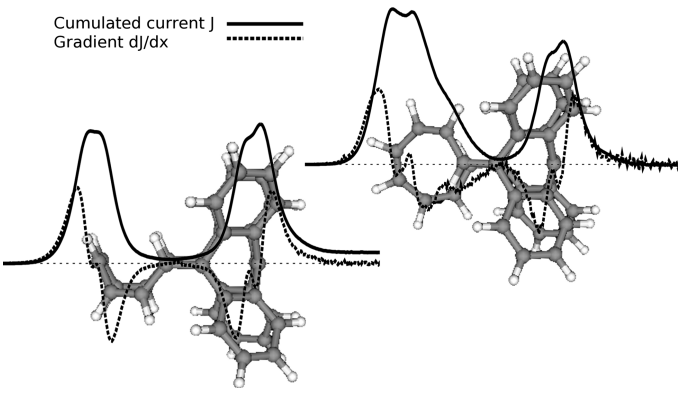

The ring currents, NMR chemical shifts, topology of the chemical bonding, and UV−vis spectra of bianthraquinodimethane-stabilized [16]annulenes possessing Möbius and Hückel topology are investigated. The aromatic character of the title compounds is discussed on the basis of the magnetically induced current density obtained using the gauge-including magnetically induced current (GIMIC) approach. Numerical integration of the current density circling around the [16]annulene ring shows that both the Hückel and the Möbius isomers are non-aromatic. The [16]annulene ring of both isomers sustains a net ring current whose strength is only 0.3 nA/T. The ring current consists of a diamagnetic flow on the outside of the [16]annulene ring and a paramagnetic current inside it. Since the net ring-current strength of the [16]annulene is less than 5% of the ring current strength for benzene, both isomers must be considered non-aromatic by the ring current criterion. The similar bond length alternation of the [16]annulene rings also points to a similarity in aromatic character of the two isomers. The shape of the ring current of the Möbius isomer shows that the current density is somewhat more outspread than that of the Hückel isomer. Spatially separated diatropic and paratropic currents of equal strength follow the annulene bonds. The atoms-in-molecules (AIM) analysis reveals a cage critical point in the region of the outspread current density of the Möbius isomer. Intramolecular CH$\cdots\pi$ and $\pi-\pi$ interactions identified by AIM analysis, in combination with the outspread current density, stabilizes the Möbius isomer relative to the Hückel one. The molecule is characterized by calculating the ^{13}C and ^{1}H NMR chemical shifts and the UV−vis spectrum and comparing these to experimental spectra. The ^{13}C NMR and ^{1}H NMR chemical shifts are rather similar for the two isomers. The UV−vis spectra are compared with the excitation energies calculated at the time-dependent density functional theory (TDDFT) level using Becke's three-parameter hybrid functional together with the LYP correlation functional (B3LYP), as well as at the approximate coupled cluster singles (CCS) and at the approximate coupled cluster singles and doubles (CC2) levels of theory. The CC2 calculations yield excitation energies in fairly good agreement with experimental data.

DOI: 10.1021/jo900736d Published on Web 08/07/2009

1. Introduction

Conjugated ring-shaped hydrocarbons with $(4n+2)$ π electrons are aromatic according to the Hückel rule,[1,2] whereas the anti-aromatic ones have a conjugation pathway consisting of $4n$ π electrons. This holds for molecules with Hückel topology having all the π orbitals oriented in the same direction. Molecules with Möbius topology on the other hand have the π orbitals twisted by 180° along the conjugation pathway around the molecular ring.[3] They are single-sided and have been suggested to be aromatic when the number of π electrons is $4n$.[4−7] The first example of a cyclic hydrocarbon with Möbius topology and $4n$ π electrons was stated to have been synthesized a few years ago[8,9] Calculations of the aromatic stabilization energy of the bianthraquinodimethane-stabilized [16]annulene indicated that it is aromatic.[8] Castro et al. reinvestigated computationally its aromaticity and concluded that it is non-aromatic on the basis of nucleus independent chemical shift (NICS) calculations.[10] In a comprehensive study of the aromaticity of a large number of [16]annulene isomers, Ajami et al. found that their bianthraquinodimethane-stabilized Möbius [16]annulene indeed exhibits aromatic properties.[11] Because of the apparent difficulties to settle this question, we employ here the gauge-including magnetically induced current (GIMIC) method[12] to calculate the strength of the ring current (susceptibility) circling around the bianthraquinodimethane-stabilized [16]annulene rings of the Möbius and Hückel isomers. The degree of aromaticity of the [16]annulenes and of the benzene rings of the bianthraquinodimethane moiety is assessed from the calculated ring-current strengths. Thus, the aromatic character of the title compound is discussed on the basis of the ring-current criterion for aromaticity: the ability of a molecule to sustain an induced net current when exposed to an external magnetic field is a necessary, though not sufficient, criterion for aromaticity.[13] An extensive study on aromatic, anti-aromatic, and non-aromatic compounds show that although aromaticity in nontrivial cases seems to be a multidimensional property, the induced ring current is often a good measure of aromaticity.[14] It was already proposed in the 1950s that ring-current strengths can be used as local and global aromaticity indices.[15]

The GIMIC method has previously been employed to calculate current strengths and current pathways of complex organic and inorganic species.[12,16−21] It has proven to be a useful tool for determining the degree of aromaticity of multiring molecules because it explicitly provides the strength of the magnetically induced current passing through selected chemical bonds and the strength of the currents circling around molecular rings. The current pathway provides information about the extent of the electron delocalization. A cyclic electron delocalization is a typical feature of aromatic molecules.

An experimental route to other candidates for aromatic molecules with Möbius topology is to synthesize expanded porphyrins[22−24] and hexaphyrins.[25−27] Extended and twisted molecular rings can also possess multiply twisted structures, rendering the aromaticity concept and the determination of the degree of aromaticity complicated.[28,29] The topology of multiply twisted objects was mathematically unravelled in the late 1960s, and very recently Rappaport and Rzepa brought these concepts into chemistry. They developed a computational approach to assess the amount of twist and writhe of multiply twisted Möbius molecules and found that the molecules either can have a twisted topology or form complicated (multi) loop structures.[30] The calculations revealed that the numbers representing the twist and the writhe are not necessarily integers, whereas the sum of the twist and writhe numbers is an integer characterizing the molecular topology and the chirality of the ring. More recently, Allan and Rzepa[31] employed the quantum theory of atoms-in-molecules (AIM) and the electron localization function to investigate a [14]annulene system. They found a pair of BCPs indicating the presence of $\pi-\pi$ interactions stabilizing the figure-eight structure of the molecule. These BCPs along with those of covalent carbon−carbon bonds contributed five ring critical points (RCPs) and two cage critical points (CCPs) that were interpreted as being associated to single-half-twist homoaromaticity and double-half-twist aromaticity. Complementary to the current-density calculations, we therefore

(1) Hückel, E. *Grundzüge der Theorie ungesättigter und aromatischer Verbindungen*; Verlag Chemie: Berlin, 1938.
(2) von Eggers Doering, W.; Detert, F. L. *J. Am. Chem. Soc.* **1951**, *73*, 876–877.
(3) Herges, R. *Chem. Rev.* **2006**, *106*, 4820–4842.
(4) Heilbronner, E. *Tetrahedron Lett.* **1964**, *5*, 1923–1928.
(5) Zimmerman, H. E. *J. Am. Chem. Soc.* **1966**, *88*, 1564–1565.
(6) Martín-Santamaría, S.; Lavan, B.; Rzepa, H. S. *J. Chem. Soc., Perkin Trans. 2* **2000**, 1415–1417.
(7) Castro, C.; Isborn, C. M.; Karney, W. L.; Mauksch, M.; Schleyer, P. v. R. *Org. Lett.* **2002**, *4*, 3431–3434.
(8) Ajami, D.; Oeckler, O.; Simon, A.; Herges, R. *Nature* **2003**, *426*, 819–821.
(9) Lemal, D. M. *Nature* **2003**, *426*, 776–777.
(10) Castro, C.; Chen, Z.; Wannere, C. S.; Jiao, H.; Karney, W. L.; Mauksch, M.; Puchta, R.; van Eikema Hommes, N. J. R.; von Ragué Schleyer, P. *J. Am. Chem. Soc.* **2005**, *127*, 2425–2432.
(11) Ajami, D.; Hess, K.; Köhler, F.; Näther, C.; Oeckler, O.; Simon, A.; Yamamoto, C.; Okamoto, Y.; Herges, R. *Chem.—Eur. J.* **2006**, *12*, 5434–5445.
(12) Jusélius, J.; Sundholm, D.; Gauss, J. *J. Chem. Phys.* **2004**, *121*, 3952–3963.
(13) Cyranski, M. K.; Krygowski, T. M.; Katritzky, A. R.; von Ragué Schleyer, P. *J. Org. Chem.* **2002**, *67*, 1333–1338.
(14) Fliegl, H.; Sundholm, D.; Taubert, S.; Jusélius, J.; Klopper, W. *J. Phys. Chem. A* **2009**, *113*, 8668–8676.
(15) Bernstein, H. J.; Schneider, W. G.; Pople, J. A. *Proc. R. Soc. London A* **1956**, *256*, 515–528.
(16) Johansson, M. P.; Jusélius, J. *Lett. Org. Chem.* **2005**, *2*, 469–474.
(17) Johansson, M. P.; Jusélius, J.; Sundholm, D. *Angew. Chem., Int. Ed.* **2005**, *44*, 1843–1846.
(18) Lin, Y. C.; Jusélius, J.; Sundholm, D.; Gauss, J. *J. Chem. Phys.* **2005**, *122*, 214308.
(19) Lin, Y. C.; Sundholm, D.; Jusélius, J.; Cui, L. F.; Li, X.; Zhai, H. J.; Wang, L. S. *J. Phys. Chem. A* **2006**, *110*, 4244–4250.
(20) Jusélius, J.; Sundholm, D. *Phys. Chem. Chem. Phys.* **2008**, *10*, 6630–6634.
(21) Taubert, S.; Jusélius, J.; Sundholm, D.; Klopper, W.; Fliegl, H. *J. Phys. Chem. A* **2008**, *112*, 13584–13592.
(22) Stepień, M; Latos-Grażyński, L; Sprutta, N; Chwalisz, P; Szterenberg, L *Angew. Chem., Int. Ed.* **2007**, *46*, 7869–7873.
(23) Herges, R. *Nature* **2007**, *450*, 36–37.
(24) Yoon, Z. S.; Osuka, A.; Kim, D. *Nat. Chem.* **2009**, *1*, 113–122.
(25) Tanaka, Y.; Saito, S.; Mori, S.; Aratani, N.; Shinokubo, H.; Shibata, N.; Higuchi, Y.; Yoon, Z. S.; Kim, K. S.; Noh, S. B.; Park, J. K.; Kim, D.; Osuka, A. *Angew. Chem., Int. Ed.* **2008**, *47*, 681–684.
(26) Sankar, J.; et al. *J. Am. Chem. Soc.* **2008**, *130*, 13568–13579.
(27) Jux, N. *Angew. Chem., Int. Ed.* **2008**, *47*, 2543–2546.
(28) Rzepa, H. S. *Org. Lett.* **2005**, *7*, 4637–4639.
(29) Rzepa, H. S. *Org. Lett.* **2008**, *10*, 949–952.
(30) Rappaport, S. M.; Rzepa, H. S. *J. Am. Chem. Soc.* **2008**, *130*, 7613–7619.
(31) Allan, C. S. M.; Rzepa, H. S. *J. Org. Chem.* **2008**, *73*, 6615–6622.

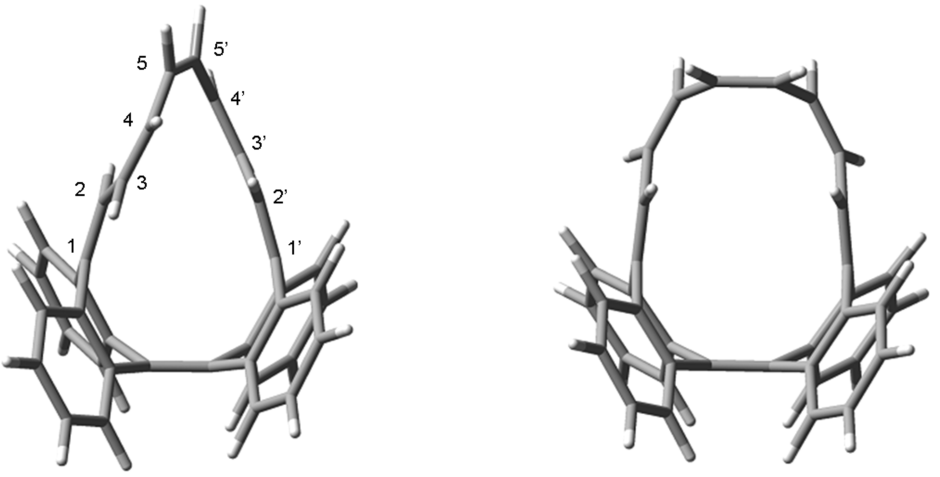

FIGURE 1. Molecular structure of the [16]annulenes with Möbius (left) and Hückel (right) topology.

performed AIM analysis on the studied [16]annulene isomers.[32]

2. Results and Discussion

2.1. Relative Stabilities. The relative stabilities of the Hückel and Möbius isomers obtained at the HF, MP2, CC2, and B3LYP levels are compared in Table 1. The molecular structures are shown in Figure 1. The methods considering electron-correlation effects predict the Möbius isomer to be the more stable one. For the Hückel and Möbius isomers, the HOMO−LUMO gaps calculated at the B3LYP/def2-TZVP level are 3.98 and 3.14 eV, respectively. Even though the strain in the twisted Möbius [16]annulene ring reduces the HOMO−LUMO gap, the Möbius isomer is lower in energy. The stabilization of the Möbius isomer with respect to the Hückel isomer going from Hartree−Fock to density functional theory (DFT) shows that electron correlation is important in these systems. The drastic lowering of the relative energy of the Möbius isomer at the MP2 and CC2 levels indicates that also London dispersion forces might be important especially in the Möbius isomer. The AIM analysis, vide infra, supports intramolecular $\pi-\pi$ interactions, which would explain the relative energy lowering at the MP2 and CC2 levels of theory. Additionally, the outspread current distribution points to an increased electron delocalization, which further would render the Möbius isomer more stable.

2.2. Magnetically Induced Currents. Calculations of the magnetically induced current density for the Möbius and Hückel isomers yield very weak ring-current strengths in the [16]annulene ring, whereas stronger current densities are obtained in the bianthraquinodimethane moieties, showing that the fused benzene rings sustain localized ring currents. The current profile along the symmetry axis in the symmetry plane are calculated to unravel the current pathways. By systematically increasing the size of the cut plane, the accumulated current strength (J) is obtained as a function of the width of the plane (x). The gradient dJ/dx calculated numerically with a five-point formula yields the shape of the current passing through the plane. The obtained current profiles are shown in Figures 2 and 3. The positive and negative peaks show the areas where the diatropic (positive) and paratropic (negative) currents dominate the current crossing the integration plane. The integrated areas under the peaks represent the strength of the current paths. The largest difference between the current density distributions of the two isomers is at the outer part of the annulene ring, where the Möbius isomer hosts a more irregular current than the Hückel isomer. The noise in the profile of the ring-current gradient in Figure 3 is due to numerical and basis set errors.

In both isomers, the fused benzene rings of the bianthraquinodimethane moiety are, by the ring-current criterion, considered as aromatic sustaining net ring currents of about 5 nA/T. This value is less than half of the benzene value because the angle between the magnetic field and the plane of the benzene ring of 57° significantly differs from 90°; the

TABLE 1. Relative Stabilities (ΔE in kJ/mol) of the Möbius and Hückel Isomers[a]

method	ΔE (kJ/mol)
HF	9.0
B3LYP	−12.6
MP2	−27.6
CC2	−31.1

[a] Negative ΔE values indicate that the Möbius isomer is more stable.

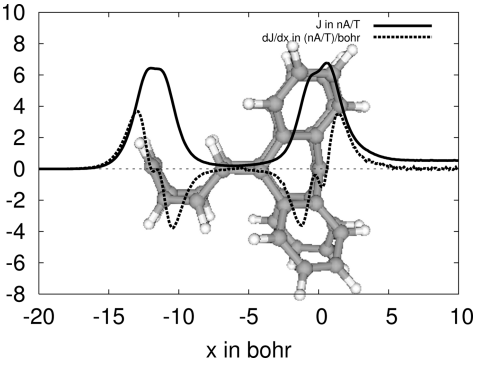

FIGURE 2. Accumulated current strength J and the ring current profile dJ/dx crossing a plane through the Hückel isomer. Positive peaks of the dashed curve represent diamagnetic currents.

(32) Bader, R. F. W. *Atoms in Molecules: A Quantum Theory*; Oxford University Press: Oxford, 1990.

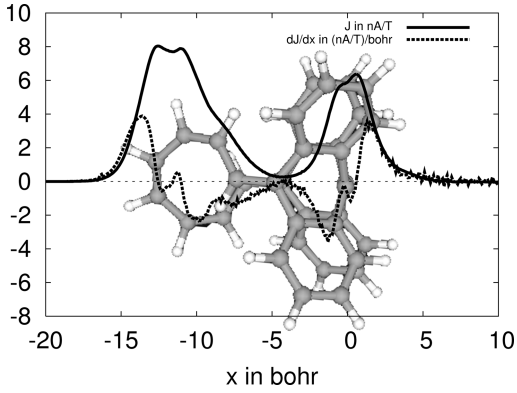

FIGURE 3. Accumulated current strength J and the ring current profile dJ/dx crossing a plane through the Möbius isomer. Positive peaks of the dashed curve represent diamagnetic currents.

maximal current is sustained when the magnetic field is perpendicular to the ring. When the magnetic field is directed perpendicularly to the plane of the benzene rings, the current strength of the benzene rings is 11.4 nA/T, which can be compared to the ring-current strength of 11.8 nA/T for an isolated benzene molecule calculated at the same level. In this sense, the electronic structure of the fused benzene rings does not differ much from that of a benzene molecule. The C=C bond of the benzene rings common to the [16]annulene is about 1 pm longer than the other bonds of the benzenes, and there is a bond length alternation of about ±0.25 pm in the rest of the benzene moiety. The current paths in the fused benzene rings are in practice decoupled from the weak current circling around the [16]annulene ring. This is in line with the observation by Castro and co-workers that benzene rings fused to annulenes cause a localization of the electrons making the annulene non-aromatic.[10]

2.3. Current Densities in the Hückel Isomer. The total current passing the outermost formal double bond of the Hückel isomer consists of paratropic and diatropic contributions. The diatropic ring current flows outside the [16]annulene ring, and the paramagnetic one circles inside it. The strengths of the diatropic and paratropic currents are about 7−8 nA/T. The almost equal strengths of the diatropic and paratropic currents are also seen as the symmetrical current profiles in the leftmost part of the molecule in Figure 2. The bianthraquinodimethane moiety hosts symmetrically distributed current densities of about 5 nA/T, as for the Möbius isomer. The ring currents are mainly localized at the individual benzene rings, whereas practically no net current circles around the [16]annulene ring. The current passing the outer edge of the [16]annulene consists of a paramagnetic component of −7.7 nA/T, and the diamagnetic component on the inside of the bond is 7.9 nA/T, resulting in a total current of 0.2 nA/T. The current passing through the formal C=C double bond across the bianthraquinodimethane group consists of a paratropic current of −6.5 nA/T on the inside. A diatropic current of 6.8 nA/T outside the [16]annulene ring yields a net current of 0.3 nA/T. According to the ring-current criterion, the [16]annulene ring of the Hückel isomer is non-aromatic. A recent study shows that non-aromatic molecules such as C_6H_8, C_6H_{10}, and C_6H_{12} sustain diatropic and paratropic ring currents with equal absolute magnitude of about 8−10 nA/T, although the total ring current practically vanishes.[14]

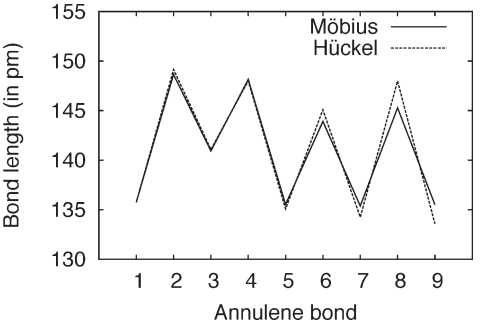

FIGURE 4. Bond-length alternation of the carbon−carbon bonds along the [16]annulene rings of the Möbius and Hückel isomers. The first bond is the formal C=C double bond between the two halves of the bianthraquinodimethane moiety.

2.4. Current Densities in the Möbius Isomer. For the Möbius isomer, the current pattern is less symmetric than for the Hückel one, as also seen in the current profile in Figure 3. This holds especially for the current density distribution inside the outer part of the [16]annulene. The current passing through a plane of size 15.0 by 20.0 bohr placed perpendicularly across the C=C bridge of the bianthraquinodimethane moiety is 0.4 nA/T, or about the same size as for the Hückel isomer. Integration of the ring current at the outermost C=C bond yields a diatropic current of 7.8 nA/T on the outside of the bond, whereas the current inside it is paratropic with a strength of −7.5 nA/T. The paratropic current inside the [16]annulene ring is more outspread than for the Hückel isomer. The carbon atoms at opposite sides of the [16]annulene are, because of the twist of the ring, somewhat closer to each other than in the Hückel isomer, enabling the current to make a through-space short cut. The through-space currents give rise to the additional peaks in the current profile in Figure 3. The net ring-current strength at the outermost C=C bond of the [16]annulene ring is 0.3 nA/T. Since the net current strength sustained by the Möbius-shaped [16]annulene ring is almost zero, it is non-aromatic by the ring-current criterion.

2.5. Bond-Length Alternation of the [16]Annulene Rings. The bond-length alternation for the [16]annulene rings can be represented by the average bond length and the deviation from the mean bond length. For the Hückel isomer, the average bond length of 143.65 ± 5.07 pm is slightly larger than the corresponding value of 143.56 ± 4.64 pm for the Möbius isomer. The bond-length alternation of the carbon−carbon bonds is displayed in Figure 4. The first carbon−carbon bond is the one across the bianthraquinodimethane moiety, and the ninth bond is the outermost bond of the [16]annulene ring. The strong bond-length alternation of both isomers indicates that the [16]annulene rings do not sustain any strong currents. The Möbius isomer has a slightly smaller bond-length alternation for the outermost carbon−carbon bonds than for the Hückel isomer. The difference is however very small, which suggests that the aromatic character of the isomers is very similar. The bond length alternation might be amplified by the benzannelation, as observed previously for the [14]annulene.[33] Both the bond-length alternation and the ring currents show that the

(33) Mitchell, R. H. *Chem. Rev.* **2001**, *101*, 1301–1315.

TABLE 2. ^{13}C and ^{1}H NMR Chemical Shifts (ppm) Calculated for the [16]Annulene Rings of the Möbius and Hückel Isomers; Experimental Values Are Given within Parentheses[8,11]

	Möbius		Hückel	
atom[a]	^{13}C	^{1}H	^{13}C	^{1}H
C_1, $C_{1'}$	147.59 (140.67)		145.04 (138.19)	
C_2, $C_{2'}$	125.90 (124.89)	6.296 (6.486)	122.39 (122.00)	6.119 (6.260)
C_3, $C_{3'}$	126.03 (127.79)	5.909 (6.118)	128.98 (128.02)	6.616 (6.624)
C_4, $C_{4'}$	127.60[b]	5.442 (5.690)	132.89 (131.52)	5.834 (5.875)
C_5, $C_{5'}$	126.96 (127.04)	5.625 (5.940)	131.61 (129.83)	6.161 (6.238)

[a]Numbering of the atoms begins at the bianthraquinodimethane moiety. See Figure 1. [b]The ^{13}C NMR chemical shift for C_4 and $C_{4'}$ has not been reported.

bianthraquinodimethane-stabilized [16]annulenes are nonaromatic.

2.6. Nuclear Magnetic Resonance Spectra. The nuclear magnetic resonance (NMR) chemical shifts calculated at the B3LYP level for the two isomers are compared to experimental values in Table 2. The ^{13}C and ^{1}H magnetic shieldings calculated for benzene at the same level are used as internal reference. The use of an internal reference compound that resembles the studied molecules improves the agreement between the calculated and measured chemical shifts.[34] At the B3LYP/def2-TZVP level, the ^{13}C NMR and ^{1}H NMR shieldings for benzene are 49.62 and 24.27 ppm, respectively. The deviations between calculated and experimental chemical shifts of the [16]annulene are as large as for benzene. The empirically corrected NMR chemical shifts are obtained as

$$\boldsymbol{\delta}_{\mathrm{calc}}(\mathrm{annulene}) = \boldsymbol{\delta}_{\mathrm{exp}}(\mathrm{benzene}) + \sigma_{\mathrm{calc}}(\mathrm{benzene}) - \sigma_{\mathrm{calc}}(\mathrm{annulene}) \quad (1)$$

where δ denotes the NMR chemical shifts and σ_{calc} are the calculated isotropic shielding constants.

The calculated and empirically corrected NMR chemical shifts agree well with the experimental values. An exception is the chemical shift of the first carbon atom (C_1) at the bianthraquinodimethane moiety; see Figure 1. For both isomers, its calculated shift is almost 7 ppm too large. In the calculations, vibrational and solvent effects are not taken into account. The vibrational corrections are not expected to be larger for C_1 than for the other carbons, whereas the solvent interactions experienced by C_1 might differ from the solvent effects of the other carbon atoms. A solvent molecule can possibly reside for a long time in the vicinity of C_1 thereby significantly affecting the experimental ^{13}C NMR chemical shift. The calculated ^{13}C NMR chemical shift for the carbons at the biantraquinodimethane bridge of the Möbius isomer is 6 ppm larger than obtained experimentally. The rest of the calculated carbon shifts are in much better agreement with the experimental values.

The trends of the calculated and measured ^{1}H NMR chemical shifts are similar. The empirically corrected ^{1}H NMR chemical shifts as reference are generally slightly smaller than those obtained experimentally. Nuclear magnetic shieldings are underestimated at the DFT level,[35] whereas cancellation of errors often render ^{1}H NMR and ^{13}C NMR chemical shifts calculated at the B3LYP level rather accurate.[35,36] The ^{13}C and ^{1}H shieldings for TMS (tetramethylsilane) calculated at the B3LYP/def2-TZVP level are 183.41 and 31.91 ppm, respectively.

2.7. AIM Analysis. The AIM analysis of the electron density, $\rho(r)$, of the Möbius isomer revealed the presence of 60 nuclear attractor critical points (NACPs), 73 bond critical points (BCPs), 15 RCPs, and one CCP, satisfying the Poincaré−Hopf theorem. Seven of the BCPs arise from the noncovalent intramolecular interactions, while the rest are concerned with the C−C and C−H covalent bonds. Six BCPs are related to CH···π interactions that arise from C−H···C contacs over distances in the range of 259−285 pm, whereas one BCP corresponds to a C···C connection of 336 pm between the C_2 and $C_{2'}$ atoms in the [16]annulene bridge, following the numbering in Figure 1. The BCP that arises from the latter interaction is located in the intraloop region, thus indicating that the annulene loop is stabilized by $\pi-\pi$ interactions.

Figure 5 shows the spatial arrangement of the CCP and the 15 RCPs in the Möbius isomer. The CCP(3,+3) is located in a region delimited by the [16]annulene loop and surrounded by four RCPs(3,+1) at the vertices of a distorted tetrahedron. This topology resembles that of tetrahedrane[32] where a CCP is surrounded by four equally spaced RCPs. In the Möbius isomer, two RCPs (a) are located 103 pm from the CCP. They are associated to a pair of rings in the upper bay region of the annulene loop, which are closed by $C_2H\cdots C_{4'}$ and $C_{2'}H\cdots C_4$ contacs, respectively, of 275 pm each. Two RCPs (b) located 96 pm below the CCP are also present. They arise from a pair of rings which are closed by CH···π interactions involving $C_2H\cdots C_{4'}$ and $C_{2'}H\cdots C_4$ contacts, respectively, along with the $C_2\cdots C_{2'}$ interaction described above. This topology differs from that of the Möbius [14]annulene molecule recently investigated by Allan and Rzepa, where two CCPs and five RCPs are present.[31]

Three other classes of RCPs are present in the Möbius isomer. One RCP (c) is located on the C_2 axis of rotation, which also contains the CCP. This central RCP(3,+1) lies 253 pm from the CCP and the distances to the carbon atoms of the three C−C bonds are between 206 and 225 pm. The central RCP is most likely associated with the HOMO-1 shown in Figure 6. The figure displays the in-phase contribution of six carbon p_π orbitals. A group of four RCPs is located in the bay regions associated to the middle (d) and bottom (e) parts of the molecule. Each pair of RCPs is associated to rings that are closed by CH···C contacts of 259 and 285 pm, respectively. Six RCPs (f) are located at the centers of the six-membered arene rings.

In contrast to the Möbius isomer, the AIM analysis of the $\rho(r)$ of the Hückel isomer yielded 11 RCPs but no CCP. In addition, 60 NACPs and 70 BCPs were obtained, as shown in Figure 5. The CPs of the Hückel isomer also satisfies the Poincaré−Hopf relation. Four of the 70 BCPs in the Hückel isomer correspond to noncovalent interactions, namely, two CH···π interactions and two H···H interactions between the CH bonds of opposing arene rings. Bader and co-workers demonstrated that these H···H interactions do have a stabilizing role in both hydrocarbon molecules and crystals

(34) Taubert, S.; Konschin, H.; Sundholm, D. *Phys. Chem. Chem. Phys.* **2005**, *7*, 2561–2569.

(35) Auer, A. A.; Gauss, J.; Stanton, J. F. *J. Chem. Phys.* **2003**, *118*, 10407.

(36) Bagno, A.; Rastrelli, F.; Saielli, G. *J. Phys. Chem. A* **2003**, *107*, 9964–9973.

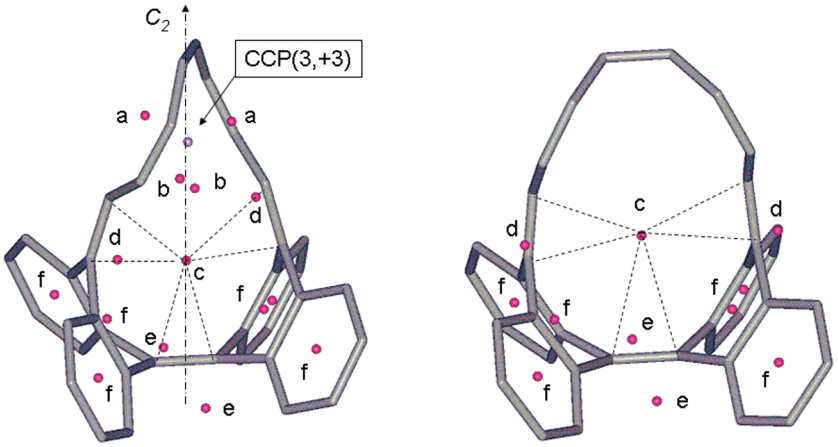

FIGURE 5. Ring and cage critical points of Möbius (left) and Hückel (right) isomers. The RCPs are categorized as follows: upper bay regions (a), intraloop region (b), central region (c), middle bay regions (d), lower bay regions (e), and six-membered arene rings (f). The dashed lines indicate the separation between six carbon atoms and the central RCP. Hydrogen atoms have been omitted for clarity.

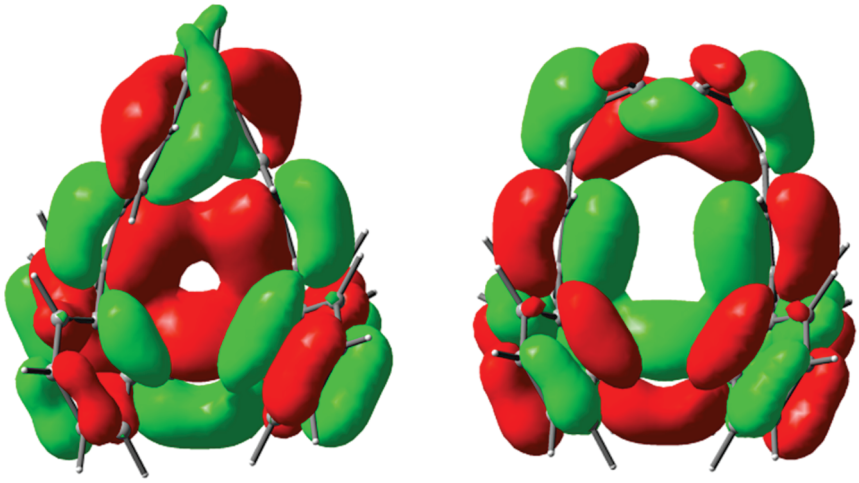

FIGURE 6. HOMO-1 of the Möbius isomer (left) and HOMO of the Hückel isomer (right) (isovalue = 0.02).

and differ from canonical dihydrogen bonds.[37] The pair of H···H interactions closing the rings characterized by the RCPs (e) of the lower bay regions are in the Möbius isomer replaced by a pair of CH···π interactions, as a consequence of the twist of the molecular skeleton under the strain provoked by the annulene loop.

It is clear from Figure 5 that, owing to the partial identity of the molecular structures, the set of 11 RCPs of the Hückel isomer match those of the Möbius isomer but the four RCPs (a,b) and the CCP associated with the annulene loop are absent in the Hückel structure. Also in the Hückel isomer, the central RCP (c) arises from the BCPs of the carbon atoms of three C−C bonds at distances ranging from 230 to 262 pm, following the dashed lines in Figure 5. This RCP is most likely associated to the HOMO shown in Figure 6. Due to the larger separation, however, the six carbon pπ orbitals do not form a delocalized central orbital as HOMO-1 of the Möbius isomer.

The presence of the CCP in the Möbius isomer and its absence in the Hückel isomer fits well with the observed current profiles. The CCP is located in the same region as the outspread current density in the Möbius isomer, while the current profile is more regular and localized for the Hückel isomer.

2.8. UV−vis Spectra. The electronic excitation spectra are calculated at the B3LYP TDDFT, CCS, and CC2 levels. The calculated and measured spectra agree well, though the calculated spectra are slightly red-shifted as compared to the experimental ones.[8,11] The few lowest excitation energies are given in Tables 3 and 4. The maxima of the experimental spectra, indicated as vertical lines in Figures 7 and 8, appear at 3.0, 4.0, and 4.9 eV for the Möbius isomer and at 4.1 and 4.8 eV for the Hückel one. At the B3LYP level, the excitation energies of the two lowest triplet states of the Möbius isomer are 1.59 eV (***B***) and 2.20 eV (***A***), and at the CC2 level they are 2.21 eV (***B***) and 2.76 eV (***A***). For the Hückel isomer, the two lowest triplet excitation energies at the B3LYP level are 2.28 eV (***A***″) and 2.31 eV (***A***′). The corresponding CC2 values are 2.94 eV (***A***′) and 2.92 eV (***A***″). The symmetry of the excited states is given within parentheses. The first singlet and triplet excitation energies of the Möbius isomer are smaller than for the Hückel one because the Möbius isomer is not significantly more aromatic than the Hückel isomer,

(37) Matta, C. F.; Hernández-Trujillo, J.; Tang, T.; Bader, R. F. W. *Chem.—Eur. J.* **2003**, *9*, 1940–1951.

TABLE 3. Lowest Excitation Energies and Corresponding Wavelengths of the Hückel Isomer Calculated at the B3LYP TDDFT, CCS, and CC2 levels[a]

	B3LYP TDDFT			CCS		CC2	
state	EE (eV)	λ (nm)	f	EE (eV)	f	EE (eV)	λ (nm)
$\mathbf{2}^1A'$	3.43	253	0.030	5.16	1.224	4.10	302
$\mathbf{1}^1A''$	3.47	358	0.006	4.44	0.002	4.04	307
$\mathbf{2}^1A''$	3.53	352	0.035	5.51	0.046	4.34	286
$\mathbf{3}^1A'$	3.86	321	0.359	5.48	0.005	4.39	283
$\mathbf{3}^1A''$	4.04	307	0.000	5.61	0.759	4.52	274
$\mathbf{4}^1A'$	4.05	306	0.036	5.64	0.030	4.60	270
$\mathbf{4}^1A''$	4.09	303	0.004	5.70	0.026	4.55	273
$\mathbf{5}^1A'$	4.12	301	0.001	5.73	0.006	4.72	263
$\mathbf{5}^1A''$	4.29	289	0.264				
$\mathbf{6}^1A'$	4.33	287	0.223				

[a] The oscillator strengths (f) are calculated at the B3LYP TDDFT and CCS levels. The maxima in the measured UV−vis spectrum are at 4.1 eV (299 nm) and 4.8 eV (259 nm).[8,11]

TABLE 4. Lowest Excitation Energies and Corresponding Wavelengths of the Möbius Isomer Calculated at the B3LYP TDDFT, CCS, and CC2 Levels[a]

	B3LYP TDDFT			CCS		CC2	
state	EE (eV)	λ (nm)	f	EE (eV)	f	EE (eV)	λ (nm)
$\mathbf{1}^1B$	2.56	485	0.074	3.60	0.103	3.09	401
$\mathbf{2}^1A$	3.48	357	0.172	4.99	1.255	3.60	344
$\mathbf{3}^1A$	3.61	344	0.025	5.46	0.041	4.01	309
$\mathbf{4}^1A$	3.69	336	0.049	5.51	0.046	4.20	295
$\mathbf{2}^1B$	3.78	328	0.048	5.39	0.410	4.35	285
$\mathbf{3}^1B$	3.91	317	0.032	5.48	0.011	4.52	274
$\mathbf{5}^1A$	4.01	309	0.002	5.70	0.001	4.24	292
$\mathbf{4}^1B$	4.05	306	0.002	5.73	0.007	4.57	271
$\mathbf{5}^1B$	4.21	294	0.001				

[a] The oscillator strengths (f) are calculated at the B3LYP TDDFT and CCS levels. The maxima in the measured UV−vis spectrum are at 3.0 eV (400 nm), 4.0 eV (312 nm), and 4.9 eV (253 nm).[8,11]

and the strain in the twisted [16]annulene ring leads to a reduction in the optical gap for the Möbius isomer. The experimental UV−vis spectrum of the Möbius isomer features two sharp peaks at 253 and 312 nm and a third broad peak with low intensity at 400 nm. The simulated spectrum constructed using the CC2 excitation energies and the B3LYP TDDFT oscillator strengths have two very strong peaks. These correspond to the singlet excitations at 285 nm ($\mathbf{2}^1\boldsymbol{B}$) and at 344 nm ($\mathbf{2}^1\boldsymbol{A}$). A third low-intensity peak originating from the singlet ($\mathbf{1}^1\boldsymbol{B}$) excitation is located at 401 nm. Following the experimental curve further toward higher energies, there is a flat area between 400 and 350 nm, which could correspond to the singlet excitations at 295 nm ($\mathbf{4}^1\boldsymbol{A}$) and 292 nm ($\mathbf{5}^1\boldsymbol{A}$) as obtained in the CC2 calculations. For the Hückel isomer, the excitation energies obtained at the CC2 level combined with the oscillator strengths calculated at the B3LYP TDDFT level reproduce well the experimental spectral features. The two peaks in the experimental spectrum at 259 and 299 nm correspond to the intense excitations in the calculated CC2 spectrum at 274 nm ($\mathbf{3}^1\boldsymbol{A}''$) and 302 nm ($\mathbf{2}^1\boldsymbol{A}'$). The combination of the CC2 excitation energies and the B3LYP band strengths works well because the character of the seven lowest states of the Möbius isomer is the same at the CC2 and B3LYP levels. For the Hückel isomer the third and the fourth excited $\boldsymbol{A}''$ and $\boldsymbol{A}'$ states are interchanged in the CC2 and B3LYP calculations. However, due to the small energy differences between the states, the reverse order does not significantly affect the shape of the simulated spectra. The excitation energies calculated at the CCS level are not very useful as correlation effects are substantial and vary from state to state.

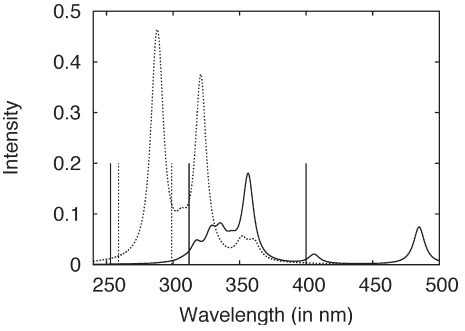

FIGURE 7. UV−vis spectra calculated at the B3LYP TDDFT level for the Möbius (solid lines) and Hückel (dashed lines) isomers. The spectra are simulated by using Lorentzian line shapes with a width of 10 nm. The absorption maxima of the experimental spectra are indicated with the vertical lines.

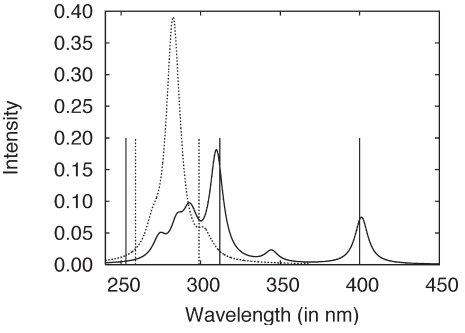

FIGURE 8. UV−vis spectra calculated at the CC2 level for the Möbius (solid lines) and Hückel (dashed lines) isomers. The B3LYP TDDFT oscillator strengths have been used together with the CC2 excitation energies. The spectra are simulated by using Lorentzian line shapes with a width of 10 nm. The absorption maxima of the experimental spectra are indicated with the vertical lines.

3. Conclusions

The magnetically induced ring-current strengths of the synthesized Möbius and Hückel [16]annulenes are studied at the B3LYP level. The calculated ring-current susceptibility of 0.3 nA/T for the [16]annulene ring of the Möbius isomer shows that it is non-aromatic by the ring-current criterion. The [16]annulene ring of the corresponding Hückel isomer equally sustains practically no ring current and is also non-aromatic. At correlated levels, the Möbius isomer is found to be 13−31 kJ/mol more stable than the Hückel one. Since the ring-current strength is equal for both isomers, the energy stabilization of the Möbius isomer most likely does not originate from the Möbius aromaticity of the [16]annulene ring. Instead, the stabilization of the Möbius isomer is presumably due to intramolecular $\pi-\pi$ interactions, as revealed by the AIM analysis. Further stabilization might originate from a slightly outspread current distribution and a through-space current in the outer bay region of the [16]annulene. The AIM analysis of the Möbius isomer also shows a cage critical point in the region where the current profile is more outspread. The AIM analysis further

indicates a stabilizing intramolecular H···H interaction in the Hückel isomer. As a combined result of these stabilizing phenomena, the Möbius isomer is energetically more favorable than the Hückel one, despite the smaller HOMO−LUMO gap and the larger strain in the [16]annulene ring of the Möbius isomer than for the Hückel one. The Hückel isomer features a more regular and localized current density distribution. For both isomers, the fused benzene rings of the bianthraquinodimethane moiety sustain an induced current that is about as strong as in a single benzene molecule, and they are thus about as aromatic as benzene.

Both isomers were investigated by calculating the NMR chemical shifts and the excitation energies, in order to compare with experimental NMR and UV−vis spectra. The ^{13}C NMR and ^{1}H NMR chemical shifts calculated at the B3LYP level agree well with experiment. The more outspread current density distribution of the Möbius isomer does not significantly affect the ^{13}C and ^{1}H NMR chemical shifts. The excitation energies calculated at the CC2 level combined with oscillator strengths obtained at the B3LYP level reproduce adequately the experimental UV−vis spectra of the Möbius and Hückel [16]annulenes. The excitation energies obtained at the B3LYP level are slightly underestimated as compared to the experiment.

4. Computational Methods

The molecular structures are optimized at the DFT level using Becke's three-parameter functional (B3LYP)[38] with the Lee−Yang−Parr correlation functional.[39] Triple-ζ quality basis sets augmented with polarization functions (def2-TZVP) are used in the structure optimizations, in the shielding calculations, and for calculating the excitation energies.[40,41] The experimental geometries[8] are used as initial structures for the optimizations. The Möbius and Hückel isomers are assumed to possess C_2 and C_s symmetry, respectively. The current densities and the ring-current susceptibilities (ring currents) are calculated at the B3LYP level employing the def-TZVP basis set.[42] The energies of the lowest singlet and triplet excited states are calculated at the time-dependent density functional theory level (TDDFT) using the B3LYP functional[43,44] as well as at the approximate singles and doubles coupled-cluster (CC2) level.[45] In the CC2 calculations, the resolution of the identity (RI) approximation is employed to speed up the calculations. Single-point energies are calculated at the Hartree−Fock (HF), second-order Møller-Plesset perturbation theory (MP2), and CC2 levels of theory. The electronic structure calculations are performed with TURBOMOLE,[46] whereas the current densities are obtained with GIMIC, which is an independent program using the perturbed and unperturbed density matrices from nuclear magnetic shielding calculations.[12] The GIMIC program is freely available on request from the authors.

The strength of the magnetically induced current circling around the [16]annulene is obtained by numerical integration of the current density passing the formal C=C double bond across the bianthraquinodimethane moiety and is compared to the current strengths passing the outer part of the [16]annulene ring. The obtained current strength depends on the direction of the applied magnetic field. Because nonplanar molecules have no obvious direction of the magnetic field, it has been chosen so that approximately the maximum projection area of the molecular wire is in a plane perpendicularly to the magnetic field. The obtained induced current strengths are used to assess the degree of aromaticity of the [16]annulene rings. In the calculations, the magnetic field is directed along the *y*-axis of Figures 2 and 3. If the magnetic field is reversed by 180°, the current strength will be the same but of opposite sign. The AIM analysis[32] of the Laplacian of the electron density $\rho(r)$ was performed with AIMAll.[47] Formatted checkpoint files of the Gaussian03[48] package were employed as input for AIMAll. In the Gaussian03 calculations, the molecular structures of the Möbius and Hückel isomers were optimized at the B3LYP/6-31G(d) level by imposing C_2 and C_s symmetry, respectively, and using the pruned ultrafine grid. The molecular orbitals were visualized with GaussView.[49]

Acknowledgment. This research has been supported by the Academy of Finland through its Centers of Excellence Programme 2006−2011 and the OPNA research project (118195). The research collaboration is supported by the Nordic Centre of Excellence in Computational Chemistry (NCoECC) project funded by NordForsk (070253). S.T. acknowledges financial support from the Alfred Kordelin Foundation. F.P. thanks the Global COE program of Tohoku University for financial support. We also thank CSC − the Finnish IT Center for Science for computer time.

Supporting Information Available: The coordinates of the investigated molecules and the full citation of ref 48 are provided in the Supporting Information. This material is available free of charge via the Internet at http://pubs.acs.org.

(38) Becke, A. D. *J. Chem. Phys.* **1993**, *98*, 5648–5652.
(39) Lee, C.; Yang, W.; Parr, R. G. *Phys. Rev. B* **1988**, *37*, 785–789.
(40) Weigend, F.; Häser, M.; Patzelt, H.; Ahlrichs, R. *Chem. Phys. Lett.* **1998**, *294*, 143–152.
(41) Weigend, F.; Ahlrichs, R. *Phys. Chem. Chem. Phys.* **2005**, *7*, 3297–3305.
(42) Schäfer, A.; Huber, C.; Ahlrichs, R. *J. Chem. Phys.* **1994**, *100*, 5829–5835.
(43) Bauernschmitt, R.; Ahlrichs, R. *Chem. Phys. Lett.* **1996**, *256*, 454–464.
(44) Furche, F.; Ahlrichs, R. *J. Chem. Phys.* **2002**, *117*, 7433–7447.
(45) Hättig, C.; Weigend, F. *J. Chem. Phys.* **2000**, *113*, 5154–5161.
(46) Ahlrichs, R.; Bär, M.; Häser, M.; Horn, H.; Kölmel, C. *Chem. Phys. Lett.* **1989**, *162*, 165–169.
(47) Keith, T. A. *AIMAll, Version 09.02.01*, **2009**. URL: http://aim.tkgristmill.com.
(48) Frisch, M. J. et al. *Gaussian 03, Revision D.02*; Gaussian Inc.: Wallingford, CT, **2004**.
(49) Dennington, R.; Todd, K.; Milliam, J. *GaussView, Version 4.1*; Semichem, Inc.: Shawnee Mission, KS, **2007**.